The Influence of Air–Sea Interaction on the Ventilated Thermocline

RICHARD G. WILLIAMS

Space and Atmospheric Physics Group, Department of Physics, Imperial College, London, UK

(Manuscript received 23 November 1988, in final form 16 March 1989)

ABSTRACT

Air–sea interaction influences the ventilated thermocline by forcing the mixed layer to deepen and cool polewards. When there is flow from the mixed layer into the interior, the mixed-layer depth and density fields help to set the potential vorticity of the subducted fluid. The importance of this process is assessed by incorporating a depth-varying mixed layer in a ventilation model which is forced by Ekman pumping and implied surface heating. The formulation of the ventilation problem is simplified by only allowing density surfaces to outcrop along latitude circles, and by assuming that there is no zonal inflow along the eastern boundary. The surface heating enables a cross-isopycnal flow within the mixed layer. The volume of ventilated fluid within the subtropical gyre is increased by including the depth-varying mixed layer, and this fluid partly originates from the western boundary, as well as from the Ekman layer. The depth-varying mixed layer increases the depth at which isopycnals are subducted and changes the value of the potential vorticity injected into the main thermocline. However, the mixed layer only alters the detail of the general streamline pattern, with an increase in the subducted potential vorticity leading to the surface flow strengthening and the deeper flow weakening.

1. Introduction

The midocean circulation has been elegantly explained in terms of a surface wind-stress curl pumping fluid from an Ekman layer, with water parcels subsequently conserving their density and potential vorticity in the stratified interior (Luyten et al. 1983; hereafter LPS). The potential vorticity q is defined, with relative vorticity neglected on the large-scale, by

$$q = -f\frac{\partial \rho}{\partial z}. \tag{1}$$

Here, f is the planetary vorticity, z is the vertical coordinate, and ρ is the density.

The potential vorticity of ventilated fluid may be expressed in terms of fluid leaving a mixed layer and entering a stratified interior (Fig. 1). The subducted isopycnals have a density difference $\Delta\rho = \rho_2 - \rho_1$ that is the same as the horizontal mixed-layer density change $\rho_m(s_2) - \rho_m(s_1)$:

$$\Delta\rho = \Delta s\frac{\partial \rho_m}{\partial s}. \tag{2}$$

Here, s is the horizontal coordinate parallel to the horizontal velocity vector $\mathbf{u}_b$, $\Delta s = s_2 - s_1$ is the horizontal change in position, and ρ_m is the vertically homogeneous mixed-layer density. The slope of the subducted isopycnals is set by the ratio of the vertical w_b and horizontal u_b velocities at the base of the mixed layer $z = -h$. For a mixed layer with uniform thickness (Fig. 1a), the vertical spacing between the subducted isopycnals $\Delta z = z(\rho_2) - z(\rho_1)$ is therefore given by

$$\Delta z = -\Delta s\frac{w_b}{u_b}. \tag{3}$$

Pedlosky et al. (1984) examine this case of a mixed layer with uniform thickness in an extension of the LPS model. The subducted potential vorticity, using (1) to (3), then depends on the planetary vorticity, the velocity field at the base of the mixed layer, and the mixed-layer density gradient:

$$q = f\frac{\mathbf{u}_b\cdot\nabla\rho_m}{w_b} \tag{4}$$

where by definition $u_b\partial\rho_m/\partial s = \mathbf{u}_b\cdot\nabla\rho_m$. The subducted potential vorticity is determined in a ventilation model after solving for the velocity field with an imposed Ekman pumping at the base of the Ekman-layer and surface heating in the mixed layer (see section 3a).

However, air–sea interaction leads to spatial variations in both depth and density of the mixed layer. In this more general case, the mixed-layer slope alters the vertical spacing Δz between the subducted isopycnals ρ_1 and ρ_2 (Fig. 1b):

$$\Delta z = -\Delta s\left(\frac{w_b}{u_b} + \frac{\partial h}{\partial s}\right). \tag{5}$$

Corresponding author address: Dr. R. G. Williams, Space and Atmospheric Physics Group, Dept. of Physics, The Blackett Laboratory, Prince Consort Road, Imperial College of Science and Technology, London SW7 2BZ, England.

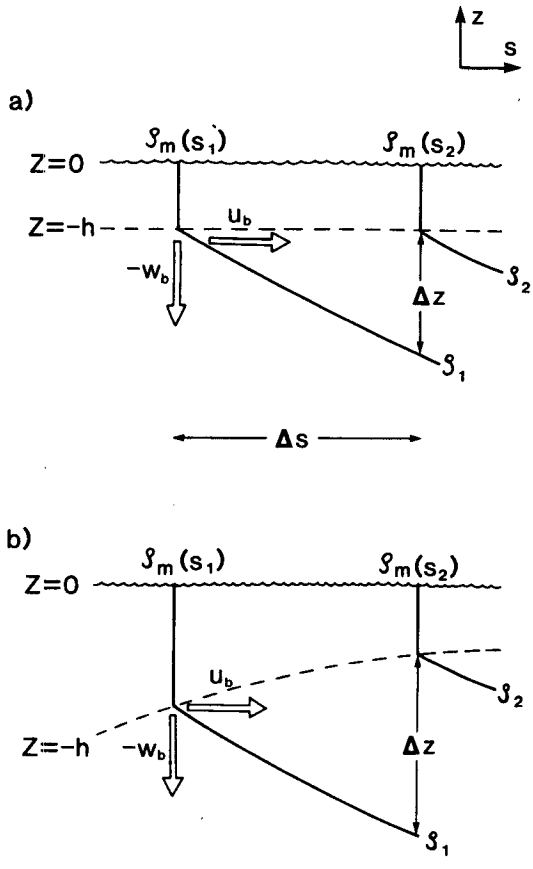

FIG. 1. Schematic diagram showing isopycnals (solid lines) subducted from (a) mixed layer (dashed line) with uniform thickness ($z = -h$), and (b) a depth-varying mixed layer, where the horizontal coordinate s is aligned parallel to the horizontal flow. The slope of the isopycnals depends on the ratio of the vertical w_b and horizontal u_b velocities at the base of the mixed layer. The vertical spacing Δz between the isopycnals depends on the mixed-layer slope, as well as the subducted isopycnal slope.

Therefore, the subducted potential vorticity now also depends on the horizontal advection through the sloping mixed layer (Woods 1985) [using (1), (2) and (5)]:

$$q = f \frac{\mathbf{u}_b \cdot \nabla \rho_m}{(w_b + \mathbf{u}_b \cdot \nabla h)}. \tag{6}$$

Air–sea interaction also produces a seasonal variation in the depth and density of the mixed-layer. The ventilating of the main thermocline is most influenced by the winter mixed layer, as fluid leaving the winter mixed layer in summer tends to be reentrained during the mixed-layer deepening in winter (Stommel 1979). In the subtropical gyre, the vertical velocity and mixed-layer depth terms in (6) typically have the same sign and magnitude assuming that $w_b \sim -30$ m yr^{-1}, the meridional velocity $v \sim -1$ cm s^{-1}, and the meridional mixed-layer slope $\partial h/\partial y \sim 100$ m/1000 km (Fig. 2). If there is the same velocity field at the base of the mixed layer, then including this sloping mixed layer over the whole gyre should lead to the subducted potential vorticity acquiring a lower value (6), than for a mixed layer with a uniform thickness (4).

These mixed-layer hypotheses of Woods and Stommel are illustrated in section 2 by considering the potential vorticity change of an advected water column (in a dynamically inactive limit) due to its seasonal mixed-layer cycle, but without including either Ekman pumping or changes in planetary vorticity.

The dynamical influence of a depth-varying mixed layer on the velocity and potential vorticity fields is then assessed using a ventilation model. A continuously stratified model developed by Huang (1988) is applied, which is an extension of the LPS model, and its controlling equations are derived in section 3. The model is used to solve for the flow in a subtropical gyre with an imposed Ekman pumping and mixed-layer field, which satisfies the requirement of no zonal flow along the eastern wall (section 4). Although the imposed mixed layer is rather artificial, the model results do show how the mixed layer alters the proportion of ventilated fluid, the density structure and the subducted potential vorticity field within the subtropical gyre (section 5).

2. Mixed-layer physics

The influence of the mixed layer on the subduction of potential vorticity is illustrated here by considering the mixed-layer cycle for a moving water column (following Woods and Barkmann 1988). A one-dimensional, Kraus–Turner (1967) type, mixed-layer model is used that solves the density and turbulent kinetic energy equations for a seasonal timescale (further details are given in Williams 1988). The model is firstly tuned for a reference site at 41°N, 27°W in the northeast Atlantic, where the net annual surface heating is close to zero, and the horizontal advection and vertical motion may be neglected (Woods and Barkmann 1986). The model is forced by diurnal solar heating and climatological monthly surface heat, water and momentum fluxes. At this reference site, the model gives a mixed-layer depth and temperature cycle which is in reasonable agreement with climatological observations of Robinson et al. (1979) (Fig. 3).

The mixed-layer model is then integrated following a water column moving from the reference site to a warmer region. For simplicity, the dynamical changes from both Ekman pumping and variations in planetary vorticity are neglected in this section. In this Lagrangian frame, the surface heating cycle is linearly increased in time from that at the reference site by an additional heating reaching 20 W m^{-2} after one year. This additional heating leads to the moving water column acquiring a shallower and warmer mixed-layer cycle, as it moves into the warmer environment (Fig. 4).

The depth of the isopycnals is initially set by the warming and rapid shallowing of the mixed layer after

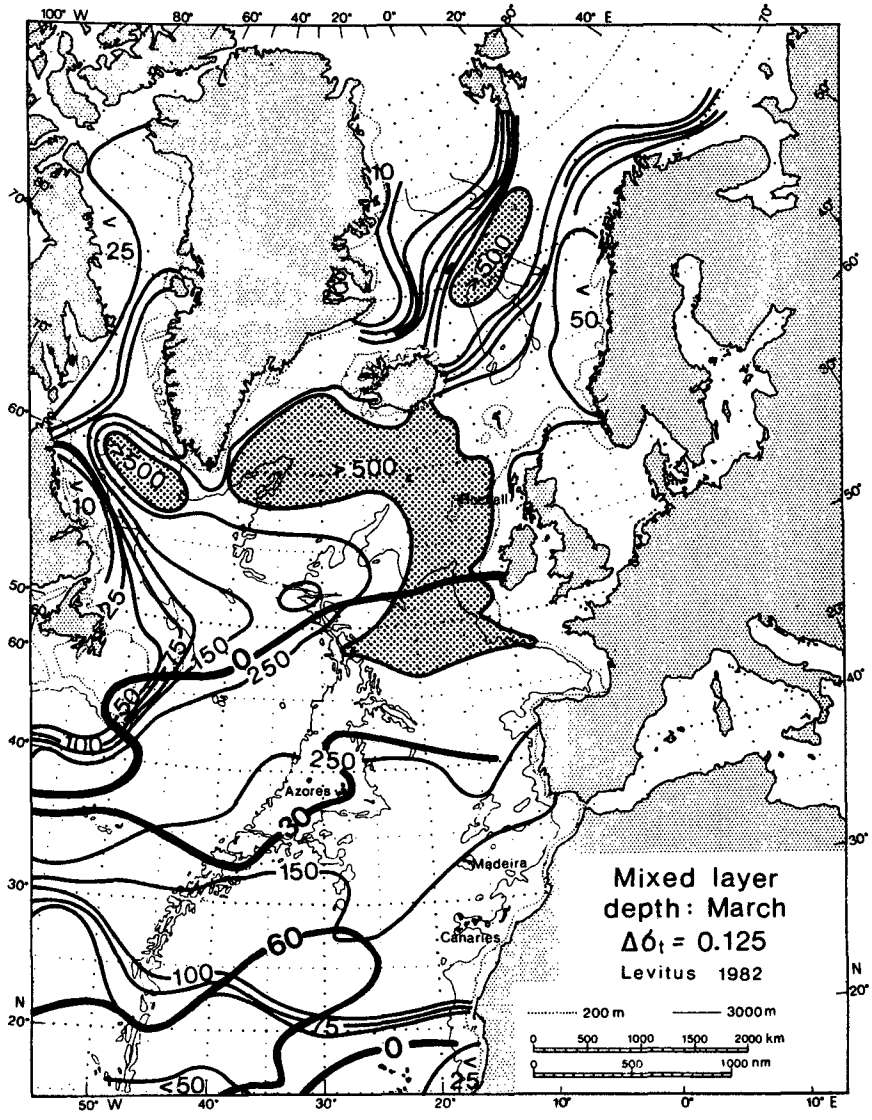

FIG. 2. Observed climatological mixed-layer depth [m] at the end of winter (thin lines) in the northeast Atlantic, and the annual mean Ekman pumping [m yr^{-1}] (thick lines) in the subtropical gyre (from Woods 1984).

the end of winter (occurring in March in Fig. 4). This leads to the potential vorticity (1) being given by the spring rates of change in the mixed-layer depth and density (Killworth, personal communication):

$$q = f \frac{\partial \rho_m}{\partial t} \Big/ \frac{\partial h}{\partial t}. \tag{7}$$

Over the following year, most of this fluid remains in the seasonal thermocline as it is reentrained by the mixed-layer deepening during the subsequent winter. However, in this warmer environment, some fluid escapes becoming reabsorbed into the mixed layer and is subducted into the main thermocline.

This subducted layer is bound by density surfaces from the mixed layer at the end of the current winter (upper surface) and the previous winter (lower surface). For example in Fig. 4, the $\sigma_t = 26.85$ layer is subducted over the first year and is bound by the $\sigma_t = 26.8$ and 26.9 surfaces. This upper bounding $\sigma_t = 26.8$ surface is now deeper, than in the previous spring, due to the effect of the additional surface heating and the background turbulent mixing. The mean potential vorticity over the subducted layer is then controlled by the winter mixed-layer gradients, rather than by the spring changes (7). In this case, if the vertical velocity is neglected in (6), then the *mean* subducted potential vorticity is given by

$$\bar{q} = f \frac{\partial \rho_m}{\partial s} \Big/ \frac{\partial h}{\partial s}. \tag{8}$$

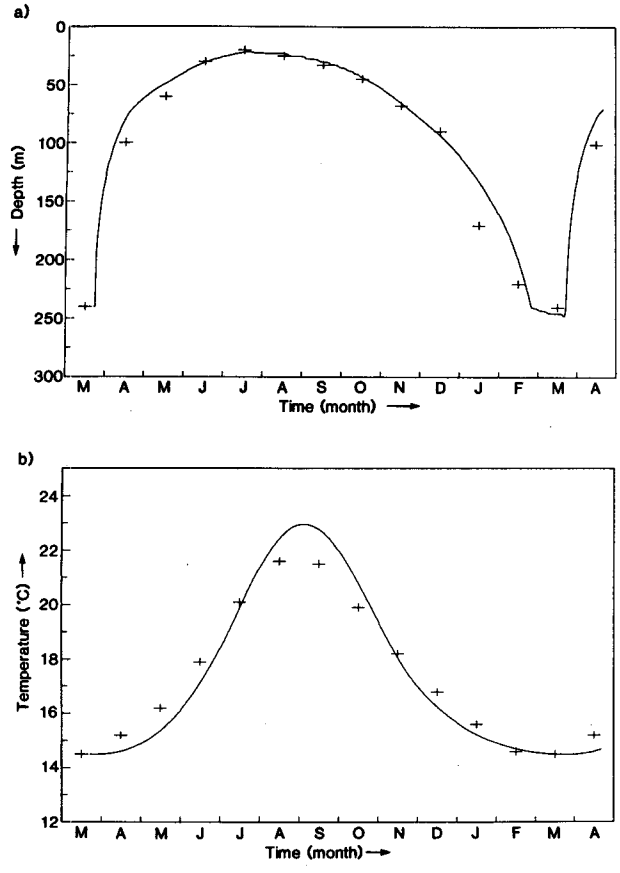

FIG. 3. Mixed-layer model cycle at a reference site 41°N, 27°W in the northeast Atlantic, where the net annual surface heating is close to zero. The daily model values of (a) mixed-layer depth, and (b) temperature (at 0600 LT), with the climatological Robinson et al. (1979) monthly observations (crosses).

These different mixed-layer processes are illustrated in Fig. 4 by the $\sigma_t = 26.85$ layer acquiring a potential vorticity of $q/\bar{\rho} = 0.06 \times 10^{-9}$ m^{-1} s^{-1} after the spring warming and shallowing of the mixed layer, but then obtains a higher value of 0.13×10^{-9} m^{-1} s^{-1} after the following winter when it is subducted into the main thermocline. The importance of the winter mixed-layer fields in setting the mean subducted potential vorticity is assessed in the following sections using a ventilation model.

However, the potential vorticity *variation* within the subducted layer entering the main thermocline is still influenced by the spring warming and rapid shallowing of the mixed layer (7). For the subducted $\sigma_t = 26.85$ layer in Fig. 4, the spring process sets the potential vorticity within the deeper and denser part of this layer. In contrast, the potential vorticity is much larger in the upper part of this layer, through the $\sigma_t = 26.8$ surface being deeper at the end of winter, than in the previous spring, and hence increasing the squashing of the underlying density surfaces. The subduction of both these spring and winter thermoclines should then lead to bands of low and high potential vorticity entering the main thermocline. In reality, this variability in the potential vorticity may help drive mesoscale eddies, which in turn should eventually smooth out these small-scale gradients.

3. Ventilation model formulation

The importance of air–sea interaction on the mid-ocean circulation is assessed by incorporating an imposed depth-varying mixed-layer in a ventilation model. The subducted potential vorticity is now set by the winter mixed-layer depth and density fields, as well as by the velocity field and the planetary vorticity (6). The ventilation model follows the continuously stratified model of Huang (1988), rather than the analytical layered model of LPS, as it allows more realistic mixed-layer density and depth changes to be incorporated.

a. Surface boundary layer

The water column consists of a shallow Ekman layer, embedded within a deeper mixed layer, and a stratified interior (Fig. 5) (Niiler and Dubbelday 1970). The velocity field is separated into an Ekman flow within the Ekman layer, and a geostrophic flow throughout the whole of the moving fluid. The surface winds drive the Ekman flow and their divergence induces a vertical velocity w_e at the base of the Ekman layer ($z = -\delta$). This Ekman upwelling drives a meridional geostrophic transport that satisfies the Sverdrup balance for large-scale flow:

$$\int_{-D}^{0} v\,dz = \frac{f}{\beta} w_e. \tag{9}$$

Here, D is the depth of the bowl of moving water, v

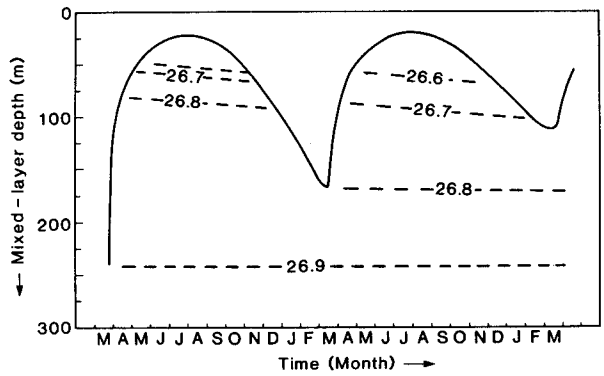

FIG. 4. Mixed-layer model cycle in a Lagrangian frame, where the water column moves from the reference site to a warmer region, showing the mixed-layer depth [m] (solid line) and the depth of the $\sigma_t = 26.6$ to 26.9 surfaces (dashed lines). Over the first year, the $\sigma_t = 26.65$ and 26.75 layers remain within the seasonal thermocline, whereas the $\sigma_t = 26.85$ layer is subducted into the main thermocline. This subducted layer is bound by the $\sigma_t = 26.9$ and 26.8 surfaces, which leave the winter mixed layer at the start and the end of the first year, respectively.

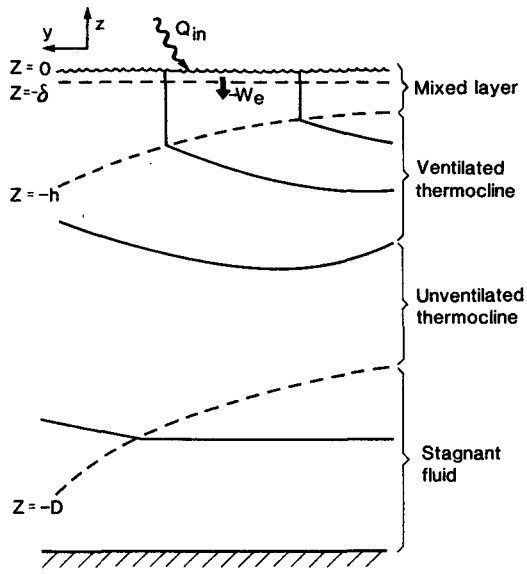

FIG. 5. Schematic north–south section showing the formulation of the ventilation model (density surfaces are solid lines, depth surfaces are dashed lines). The water column is separated into a shallow Ekman layer ($z = -\delta$), within a deeper mixed layer ($z = -h$), and with a stratified interior. The Ekman upwelling w_e and the surface heating Q_{in} drive a diabatic flow in the mixed layer and an adiabatic flow in the bowl of moving water ($z = -D$).

the meridional geostrophic velocity, and β the planetary-vorticity gradient. In the mixed layer, the geostrophic balance is given by

$$u_m = -\frac{1}{\bar{\rho} f}\frac{\partial P}{\partial y}, \quad v_m = \frac{1}{\bar{\rho} f}\frac{\partial P}{\partial x} \tag{10}$$

and the depth-integrated hydrostatic balance by

$$P(x, y, z) = P_s(x, y) - \rho_m g z. \tag{11}$$

Here, g is gravity, P_s the surface pressure field, P the depth-varying pressure field, u the zonal geostrophic velocity, and $\bar{\rho}$ a reference density.

Diabatic heating leads to cross-isopycnal flow in the vertically homogeneous mixed layer. For an annual mean steady state, there is a local balance between the net surface heat flux Q_{in} into the mixed layer and the horizontal advection by the Ekman $\mathbf{u}_e$ and geostrophic $\mathbf{u}_m$ flows:

$$\int_{-\delta}^{0} \mathbf{u}_e \cdot \nabla \rho_m dz + \int_{-h}^{0} \mathbf{u}_m \cdot \nabla \rho_m dz = -\frac{\alpha}{C_w} Q_{in}. \tag{12}$$

Here, α is the density expansion coefficient for temperature, and C_w is the heat capacity for seawater.

The vertical velocity w_b at the base of the mixed layer (Fig. 1) drives the geostrophic flow in the stratified interior, and depends on the Ekman upwelling velocity and the meridional geostrophic transport in the mixed layer [which is controlled by the surface heating from (12)]:

$$w_b = w_e - \int_{-h}^{0} \frac{\beta v}{f} dz. \tag{13}$$

b. Stratified interior

In the stratified interior, there is no diabatic forcing and water-parcels conserve their density and potential vorticity. In this region, the controlling equations are written in isopycnal coordinates using the Montgomery potential:

$$M(x, y, \rho) = P(x, y, z) + \rho g z. \tag{14}$$

The geostrophic and hydrostatic equations become

$$u_i = -\frac{1}{\bar{\rho} f}\frac{\partial M}{\partial y}, \quad v_i = \frac{1}{\bar{\rho} f}\frac{\partial M}{\partial x} \tag{15}$$

and

$$\frac{\partial M}{\partial \rho} = g z. \tag{16}$$

The potential vorticity (1) is related to the Montgomery potential in isopycnal coordinates by

$$\frac{\partial^2 M}{\partial \rho^2} = -\frac{fg}{q}. \tag{17}$$

c. Boundary conditions

The controlling equations (9) to (17) may be solved given appropriate upper, lower and lateral boundary conditions. The lower boundary condition requires that there is no flow at the base of the moving water (where $\rho = \rho_d$ and $z = -D$). Continuity of pressure and the depth of isopycnals implies that the Montgomery potential and its density gradient become the same as the abyssal values (denoted by subscript a), which may be written as

$$M(\rho_d) = M_a, \quad \frac{\partial}{\partial \rho} M(\rho_d) = \frac{\partial}{\partial \rho} M_a. \tag{18}$$

The density and pressure are continuous across the interface between the mixed layer and the stratified interior. Applying (11) and (14) then gives the matching boundary condition that the surface pressure is the same as the Montgomery potential at the base of the mixed layer:

$$M(\rho_m) = P_s. \tag{19}$$

At this interface, the mixed-layer depth is related to the Montgomery potential from the hydrostatic relation (16) by

$$\frac{\partial}{\partial \rho} M(\rho_m) = -gh. \tag{20}$$

In contrast, the LPS and Huang models assume that the mixed-layer depth is the same as a uniform Ekman depth (which is set to zero in their coordinate system).

The eastern boundary is assumed to be a wall with no inflow at each depth level. This leads to the bowl of moving water surfacing on the eastern wall (at x_e), producing an artificial singularity in potential vorticity, and the Montgomery potential satisfying

$$M(x_e) = M_a, \quad \frac{\partial}{\partial \rho} M(x_e) = \frac{\partial}{\partial \rho} M_a. \tag{21}$$

In the mixed layer, there is no geostrophic flow into the wall, which requires that the mixed-layer depth becomes zero on the eastern wall. This boundary condition is a severe constraint on the possible stratification and the resulting velocity field. In the LPS model, this leads to the deepest ventilated layer having a stagnant, shadow zone and the upper ventilated layers having zero thickness on the wall.

A less restrictive boundary condition is that there is no depth-integrated inflow on the eastern wall (Pedlosky 1983). This requirement leads to a surface geostrophic inflow and a deeper compensating outflow. However, the potential vorticity of this outflow needs to be arbitrarily chosen, which significantly alters the baroclinic flow in the interior: Pedlosky obtains stagnant, shadow zones extending from the eastern boundary in each layer. In this study, we choose to apply the LPS boundary condition in order to concentrate on the potential vorticity change from the mixed layer, rather than that from the eastern boundary. Further work is clearly necessary in order to have a more realistic stratification on the eastern wall.

The western boundary, on the other hand, is simply chosen to passively inject the required fluid to satisfy the ventilated solutions. In reality, the western boundary influences the interior by setting the potential vorticity of unventilated fluid and by helping to control the outcropping of density surfaces. Unventilated fluid does not pass through the mixed layer and is assumed to have homogenized potential vorticity in accord with the eddy diffusion arguments of Rhines and Young (1982), and Marshall and Nurser (1986): this fluid is either denser than the ventilated layer or is within the recirculation "pool" along the western side of the gyre.

d. Sverdrup balance

The Sverdrup equation (9) may be written as a balance between the Ekman upwelling and the meridional transports within (i) the mixed layer, and (ii) the stratified interior:

$$\int_{-h}^{0} v_m dz + f \int_{\rho_m}^{\rho_d} \frac{v_i}{q} d\rho = \frac{f}{\beta} w_e. \tag{22}$$

The geostrophic transport in the mixed layer is given by invoking (10) and (11):

$$\int_{-h}^{0} v_m dz = \frac{1}{\bar{\rho} f}\left(h \frac{\partial P_s}{\partial x} + \frac{1}{2} g h^2 \frac{\partial \rho_m}{\partial x}\right). \tag{23}$$

The transport in the stratified interior is obtained by invoking (15) and (17), and integrating by parts:

$$f \int_{\rho_m}^{\rho_d} \frac{v_i}{q} d\rho = -\frac{1}{\bar{\rho} f g}\left\{\left[\frac{\partial M}{\partial x}\frac{\partial M}{\partial \rho}\right]_{\rho_m}^{\rho_d} - \frac{1}{2}\int_{\rho_m}^{\rho_d} \frac{\partial}{\partial x}\left(\frac{\partial M}{\partial \rho}\right)^2 d\rho\right\}. \tag{24}$$

Applying the upper and lower boundary conditions (18) and (20) implies that

$$\left[\frac{\partial M}{\partial x}\frac{\partial M}{\partial \rho}\right]_{\rho_m}^{\rho_d} = gh \left.\frac{\partial M}{\partial x}\right|_{\rho_m}. \tag{25}$$

This horizontal gradient may be transformed from isopycnal to depth coordinates, and then applying relations (19) and (20) gives

$$\left.\frac{\partial M}{\partial x}\right|_{\rho_m} = \frac{\partial P_s}{\partial x} + gh \frac{\partial \rho_m}{\partial x}. \tag{26}$$

The Sverdrup transport (22) may be evaluated using (23) to (26), and rewritten using the hydrostatic equation $\partial M/\partial \rho = gZ$, thus

$$\frac{g}{2\bar{\rho} f}\left\{-h^2 \frac{\partial \rho_m}{\partial x} + \int_{\rho_m}^{\rho_d} \frac{\partial}{\partial x} Z^2 d\rho\right\} = \frac{f}{\beta} w_e. \tag{27}$$

If written this way, the Ekman upwelling balances the transports associated with (i) the shear within the mixed layer from its horizontal density gradient, and (ii) the shear from the deformation of the interior density field (with an Ekman pumping leading to a southwards flow and isopycnals deepening westwards).

Integrating the Sverdrup equation (27) from the eastern wall along latitude circles, applying the no inflow boundary condition on the eastern wall [$\rho_d(x_e) = \rho_m(x_e) = \rho_0$], and rearranging gives

$$\int_{\rho_m}^{\rho_d} Z^2 d\rho + \int_{x}^{x_e} Z^2(\rho_d) \frac{\partial \rho_d}{\partial x} dx = -\frac{2\bar{\rho} f^2}{g\beta} \int_{x}^{x_e} w_e dx. \tag{28}$$

The mixed-layer term in (27) is now absorbed within the first integral in (28), and the second integral in (28) may be rewritten in terms of the vertical position Z_e of isopycnals on the eastern wall:

$$\int_{x}^{x_e} Z^2(\rho_d) \frac{\partial \rho_d}{\partial x} dx = \int_{\rho_d(x)}^{\rho_d(x_e)} Z_e^2 d\rho. \tag{29}$$

Then, the zonally integrated Sverdrup equation (28) becomes

$$\int_{\rho_m}^{\rho_d} Z^2 d\rho - \int_{\rho_d(x_e)}^{\rho_d(x)} Z_e^2 d\rho = -\frac{2\bar{\rho} f^2}{g\beta} \int_{x}^{x_e} w_e dx. \tag{30}$$

Now, the zonally integrated Ekman upwelling balances the integrated transport due to the difference between the shears from the deformation of the interior density field and that on the eastern wall. This is clearly analogous to the LPS forcing equation (2.9):

$$H^2 - H_e^2 = -\frac{2\bar{\rho}f^2}{g\beta\Delta\rho}\int_x^{x_e} w_e dx$$

where H and H_e are the depths of the ventilated layer in the interior and on the eastern wall, and $\Delta\rho$ is the density difference between the LPS density layers.

Following Huang, the zonally integrated Sverdrup equation (30) may be further modified for technical convenience to help obtain ventilated solutions. The deep unventilated fluid (with $\rho_d \geq \rho \geq \rho_0$) is assumed to have homogenized potential vorticity $q_0 = -f_0 d\rho_a/dz$, where f_0 is the planetary vorticity along the northern edge of the subtropical gyre and $d\rho_a/dz$ is the abyssal stratification. Integrating the potential vorticity relation (17) in this homogenized potential vorticity layer (from the base of the ventilated layer, which has a density ρ_0 and a vertical position Z_0) gives

$$Z = Z_0 - \frac{f}{q_0}(\rho - \rho_0). \tag{31}$$

Then, applying the no flow boundary condition on the eastern wall (21) and ensuring continuity in the depth of isopycnals leads to

$$Z_0 = -\frac{f_0}{q_0}(\rho_d - \rho_0)\left(1 - \frac{f}{f_0}\right)$$

$$Z_e = -\frac{f_0}{q_0}(\rho - \rho_0). \tag{32}$$

The zonally integrated Sverdrup equation (30), after substituting (31) and (32), becomes

$$\int_{\rho_m}^{\rho_0} Z^2 d\rho + \frac{q_0 Z_0^3}{3f}[1 - (1 - f/f_0)^{-2}] = -\frac{2\bar{\rho}f^2}{g\beta}\int_x^{x_e} w_e dx. \tag{33}$$

This is the key equation to be solved in order to obtain ventilated solutions.

4. Method of solution

Ventilated solutions are obtained in the subtropical gyre by imposing the Ekman pumping, the mixed-layer depth and density fields, and deducing the required surface heating. The Ekman pumping is chosen to vary sinusoidally with latitude over a rectangular basin, extending from 15° to 48°N, 68° to 15°W:

$$w_e = -w_0 \sin(\gamma y). \tag{34}$$

Here, w_0 is the maximum Ekman upwelling, y is zero on the southern boundary and equals y_n on the northern boundary, and $\gamma = \pi/y_n$.

The mixed-layer density is chosen to vary linearly with latitude from $\sigma_t = 25.8$ to 27.0 on the southern and northern boundaries, and to outcrop along latitude circles. In contrast, Pedlosky et al. (1984) more realistically allow the surface heat balance to determine the outcropping pattern (although with a uniform mixed-layer thickness). The model parameters are chosen to roughly correspond to observations of the subtropical gyre (Table 1).

The imposed mixed-layer depth has to vanish on the eastern wall in order to satisfy the no inflow boundary condition. As there is no Ekman pumping on the northern and southern boundaries, the mixed-layer depth also has to have the same value as on the eastern wall. In addition, the mixed-layer slope is limited by the method of solution requiring that there is a southwards flow throughout the bowl for Ekman pumping: if the mixed-layer depth increased too rapidly westwards, there would have to be an underlying northwards flow in order to satisfy the Sverdrup balance. The mixed-layer depth is chosen to satisfy these constraints and vary in the following way:

$$h(x, y) = h(y)(1 - x/L)^{1/2} \tag{35}$$

where $h(y)$ varies from zero on the northern and southern boundaries to a maximum interior value of 275 m (Fig. 6), and L is the lateral extent of the gyre. This imposed mixed-layer depth field is still rather artificial compared with the observed variation (Fig. 2), and so the model is most useful for comparison with other thermocline models, such as the LPS layered model, the continuous version by Huang, or the similarity solution approach of Killworth (1987).

In the model, the ventilated fluid is separated into discrete density layers that outcrop into the mixed layer. Following Huang, the model integration is started at the most northern outcropping surface within the subtropical gyre (Fig. 7a), with only a single ventilated density layer. The vertical position Z_0 of the base of the ventilated layer is obtained at each gridpoint by solving the zonally integrated Sverdrup balance (33):

TABLE 1. Model parameters.

Variable	Symbol	Value
Maximum Ekman upwelling	w_0	60 m yr^{-1}
Zonal extent	L	5000 km
Meridional extent	y_n	3670 km
Maximum mixed-layer depth	h	275 m
Homogenized potential vorticity	$q_0/\bar{\rho}$	1.0×10^{-10} m^{-1} s^{-1}
Relative meridional positions:		
maximum mixed-layer depth	y_h/y_n	0.74
maximum Sverdrup transport	y_{sv}/y_n	0.59
maximum Ekman pumping	y_{ek}/y_n	0.50

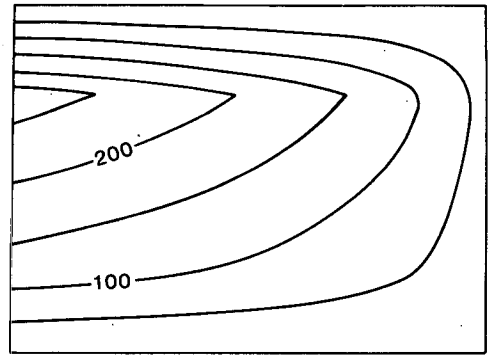

FIG. 6. The imposed mixed-layer depth field [m], which is constrained to be zero on the eastern wall in order to satisfy the no inflow boundary condition.

$$\int_{\rho m}^{\rho 0} Z^2 d\rho + \frac{q_0 Z_0^3}{3f}\left[1-(1-f/f_0)^{-2}\right] = -\frac{2\bar{\rho} f^2}{g\beta}\int_x^{x_e} w_e dx.$$

In this ventilated density layer (Fig. 7b), the Montgomery potential M_1 is obtained by ensuring continuity in M along the interface between the ventilated and unventilated fluid [integrating relations (31) and (32), and applying the no flow eastern boundary condition (21)] to give

$$M_1 = \frac{g}{2}\left(\frac{q_0 Z_0^2}{(f_0 - f)} - \Delta\rho Z_0\right). \tag{36}$$

The subducted potential vorticity is deduced from the vertical spacing between the mixed layer and the underlying density surface:

$$q_k = f\frac{\Delta\rho}{|Z_{k-1}| - h}. \tag{37}$$

Here, the vertical position of the underlying density surface is Z_{k-1}, k is a vertical counter, and $\Delta\rho$ is the density difference between the ventilated density layers. The functional relationship between the Montgomery potential M_1 and the potential vorticity q_1 is then set for this density surface.

The integration is continued further south along every outcrop surface in the gyre and an iterative approach is applied at each gridpoint:

(i) the vertical position Z_0 of the base of the ventilated-layer is estimated,

(ii) this is related to the Montgomery potential M_1 in the deepest ventilated density layer by applying the lower boundary condition (36),

(iii) the Montgomery potential for shallower density layers is obtained by integrating upwards using (17)

$$\frac{\partial^2 M}{\partial \rho^2} = -\frac{fg}{q}$$

where the relationship between M and q for each ρ surface is found according to their values subducted at a higher latitude (Fig. 7c) (like LPS, this applies the conservation of q and ρ along trajectories for adiabatic flow); any shallow unventilated fluid (with $\rho \leqslant \rho_0$) that does not pass through the mixed layer is assumed to have the same q as on the most western, ventilated trajectory for that density surface (this is the western "pool" region of the LPS solutions),

(iv) the implied transports are calculated from the Montgomery potential field and are compared with the zonally integrated Sverdrup balance (33), if this constraint is not satisfied, then the choice in the depth of the ventilated layer is adjusted and the process is repeated,

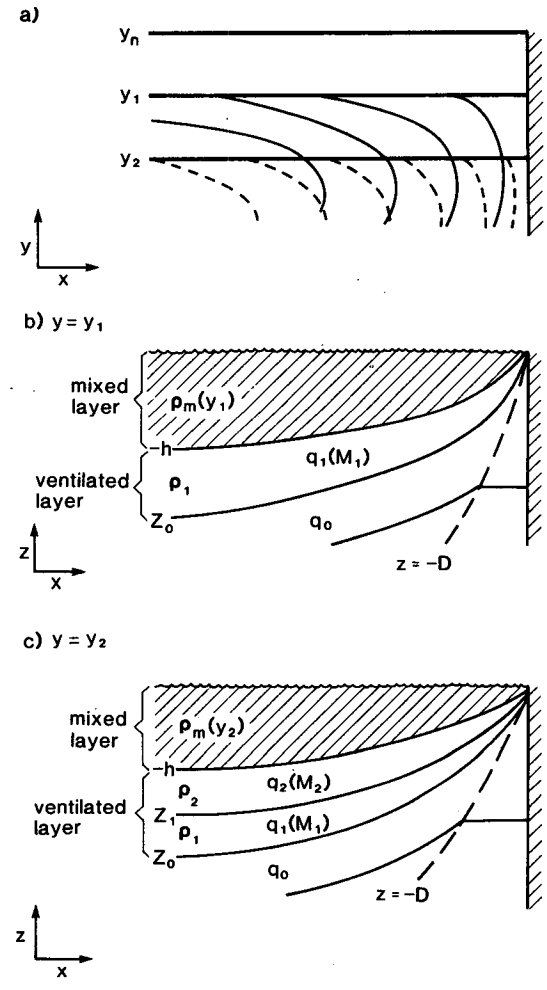

FIG. 7. Schematic diagram illustrating the method of solution: (a) a plan view of the subtropical gyre, showing the northern outcropping density surfaces along y_1 and y_2 (thick solid lines) with their streamlines (thin solid and dashed lines), (b) a vertical section at y_1, where the q_1 and M_1 values for the ρ_1 layer are obtained after solving the Sverdrup equation, (c) a vertical section at y_2, where the q_2 and M_2 values for the ρ_2 layer are obtained after solving the Sverdrup equation and using the functional relationship between q_1 and M_1.

(v) the potential vorticity subducted at this outcrop is deduced from the upper boundary condition (37), which again sets the functional relationship between M and q for this density surface,

(vi) the implied heat input (12) is finally deduced from the meridional cross-isopycnal flow in the surface boundary layer,

$$\left(\int_{-\delta}^{0} v_e dz + \int_{-h}^{0} v_m dz\right) \frac{d\rho_m}{dy} = -\frac{\alpha}{C_w} Q_{\text{in}} \quad (38)$$

where the imposed meridional Ekman volume flux per unit length is given by

$$\int_{-\delta}^{0} v_e dz = \frac{w_0}{\gamma} \cos(\gamma y).$$

5. Ventilation model results

a. *Partition of flow*

The moving fluid in the subtropical gyre may be separated into that originating from the Ekman layer and that from the western boundary. The volume flux from the Ekman layer into the subtropical gyre is given by

$$F_e = -\int_0^{y_n} \int_0^{x_e} w_e dx dy. \quad (39)$$

The volume flux from the western boundary is given by

$$F_w = \int_{-D}^{0} \int_{y_*(z)}^{y_n} u_w dy dz. \quad (40)$$

Here, the zonal inflow $u_w(y, z)$ from the western boundary vanishes at a position $y_*(z)$ along the western edge of the gyre.

The ratio of the flux from the Ekman layer to the total flux into the whole gyre is given by the recirculation index:

$$R_c = \frac{F_e}{F_e + F_w}. \quad (41)$$

The recirculation index varies principally with the planetary vorticity change across the gyre and the pattern of the wind-forcing. In this study, the recirculation index is only O(2/5) with the Ekman flux smaller than the flux from the western boundary (Table 2); here, a beta-plane approximation and a sinusoidal wind-forcing are applied.

TABLE 2. Partition of flow in the subtropical gyre.

Volume flux into the gyre	Variable	Value (10^6 m^3 s^{-1})
Ekman pumping flux	F_e	22
Western boundary flux	F_w	33
Total flux	$F_e + F_w$	55
Ventilated flux	$F_e + R_m F_w$	30
Unventilated flux	$(1 - R_m)F_w$	25

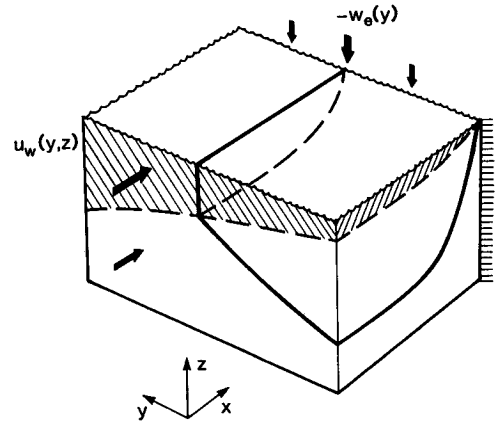

FIG. 8. Schematic diagram showing the partition of the western inflow in the subtropical gyre. The flow from the western boundary $u_w(y, z)$ may be separated into ventilated fluid, which passes through the mixed layer (dashed line) and has its potential vorticity set upon leaving it, and unventilated fluid that has its potential vorticity set by the western boundary.

Rhines (1986) therefore argues that LPS overemphasize the importance of the ventilated fluid origi-

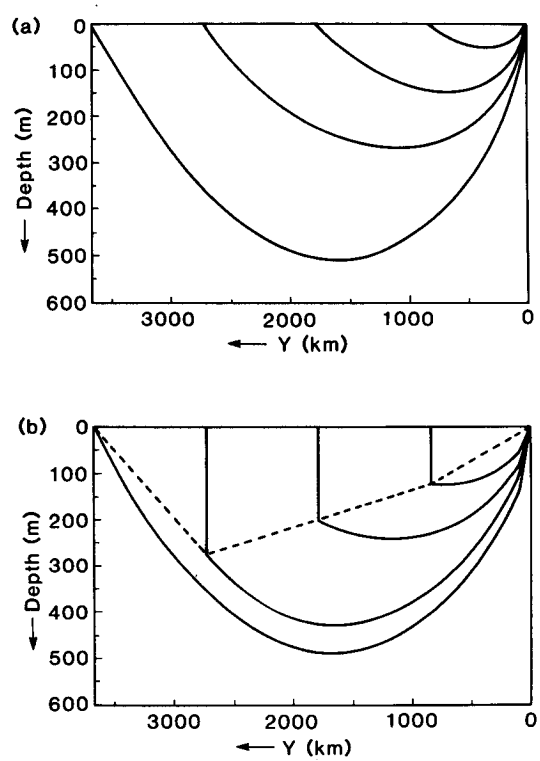

FIG. 9. North–south section showing the depth of the σ_t = 27.0, 26.7, 26.4 and 26.1 surfaces (solid lines) within the ventilated layer along the western edge of the subtropical gyre with (a) no mixed layer, and (b) a depth-varying mixed layer (dashed line). The deepest isopycnal shown is at the base of the ventilated layer.

nating from the Ekman layer, as most of the moving fluid in fact comes from the western boundary. However, when there is a depth-varying mixed layer, ventilated fluid partly comes from the western boundary, as well as from the Ekman layer. The ventilated proportion of the zonal inflow that passes through the mixed layer (Fig. 8) is given by

$$R_m = \int_{-h}^{0}\int_{y_*(z)}^{y_n} u_w dydz \Big/ \int_{-D}^{0}\int_{y_*(z)}^{y_n} u_w dydz \quad (42)$$

with the imposed mixed-layer depth being a maximum along the western edge of the gyre.

This ratio varies almost linearly with changes in the imposed mixed-layer depth, and is O(1/4) for a maximum mixed-layer depth of 275 m. Consequently, the ventilation ratio now becomes different to the recirculation index (41) and is given by

$$R_v = \frac{F_e + R_m F_w}{F_e + F_w}. \quad (43)$$

The ventilation ratio becomes O(11/20) here, and this fraction of the total flow into the gyre passes through the mixed layer and has its potential vorticity set upon leaving it (Table 2).

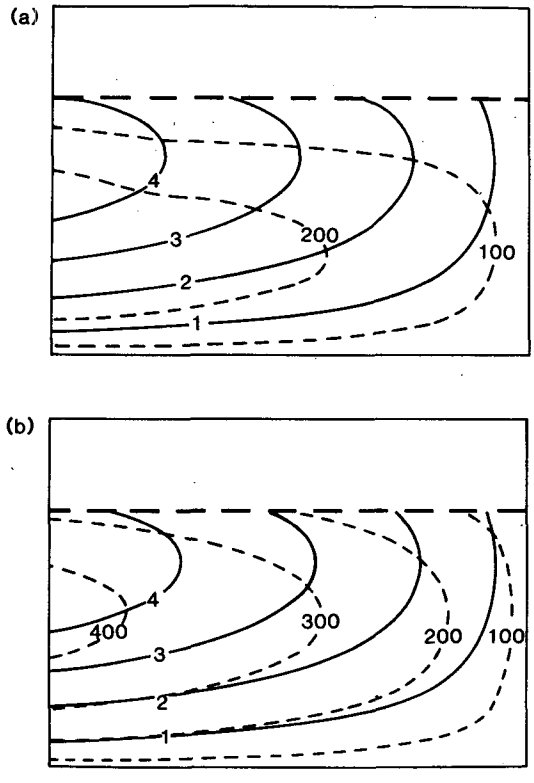

FIG. 10. Perturbation Montgomery potential (solid line) [10^3 N m^{-2}] and depth contours (dashed line) [m] along the σ_t = 26.7 surface in the ventilated layer of the subtropical gyre with (a) no mixed layer, and (b) a depth-varying mixed layer.

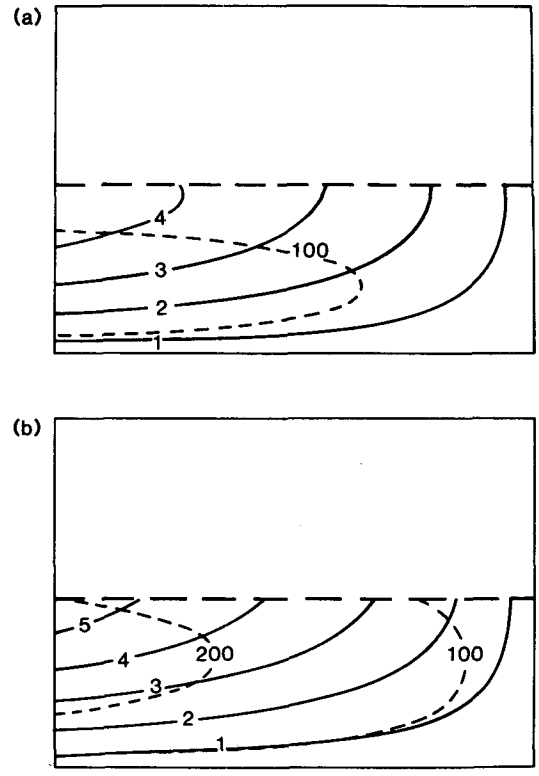

FIG. 11. As in Fig. 10, except for the σ_t = 26.4 surface.

b. *Ventilated layer results*

In the subtropical gyre, the Ekman pumping drives a southwards Sverdrup transport and forces the ventilated layer to dome downwards reaching a maximum depth along the western edge of the center of the gyre. In the LPS and Huang models, isopycnals outcrop at the surface (or into a mixed layer with uniform thickness), whereas more realistically they outcrop into a depth-varying mixed layer (Fig. 9). In the depth-varying case, the isopycnals are subducted at much greater depths within the ventilated layer, although the depth of the moving fluid and the base of the ventilated layer (deepest isopycnal shown in Fig. 9) become slightly shallower in compensation. This leads to a net "squashing" of isopycnals, which increases the subducted potential vorticity by typically up to a factor of 2 within the ventilated layer.

The general streamline pattern shows a western inflow into the northern part of the subtropical gyre, and an outflow from the rest of the gyre. The Montgomery potential field along the subducted density surfaces is hardly changed by the depth-varying mixed layer, even though the depth of the density surfaces is increased by typically 100 m (Figs. 10 and 11). The Montgomery potential increases westwards along the subducted density surfaces, whereas the potential vorticity gen-

erally decreases westwards away from an infinite value on the eastern wall. The depth-varying mixed layer alters their functional relationship by increasing the value of the subducted potential vorticity (Fig. 12); in fact, the imposed mixed layer deepens westwards so rapidly along the $\sigma_t = 26.7$ surface that the potential vorticity unusually increases westwards along part of this surface.

The depth-varying mixed layer alters the baroclinic flow by increasing the depth of isopycnals within the ventilated layer. This increases the vertical shear, which strengthens the surface flow and in compensation weakens the deeper flow (Fig. 13). The surface flow

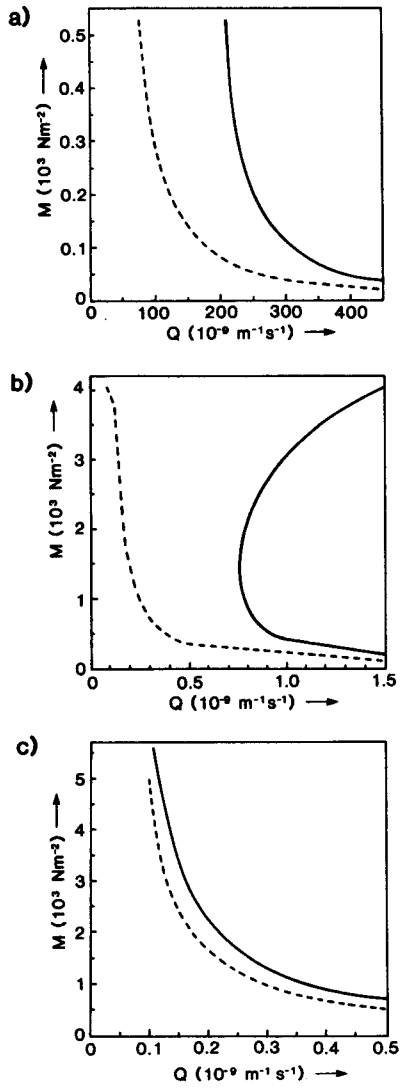

FIG. 12. Perturbation Montgomery potential [N m^{-2}] and potential vorticity $Q = q/\bar{\rho}$ [m^{-1} s^{-1}] relationship with no mixed layer (dashed line) and a depth-varying mixed layer (full line) along (a) $\sigma_t = 26.98$, (b) $\sigma_t = 26.7$, and (c) $\sigma_t = 26.4$ surfaces, which outcrop at $y/y_n = 0.98$, 0.75 and 0.5 in the subtropical gyre.

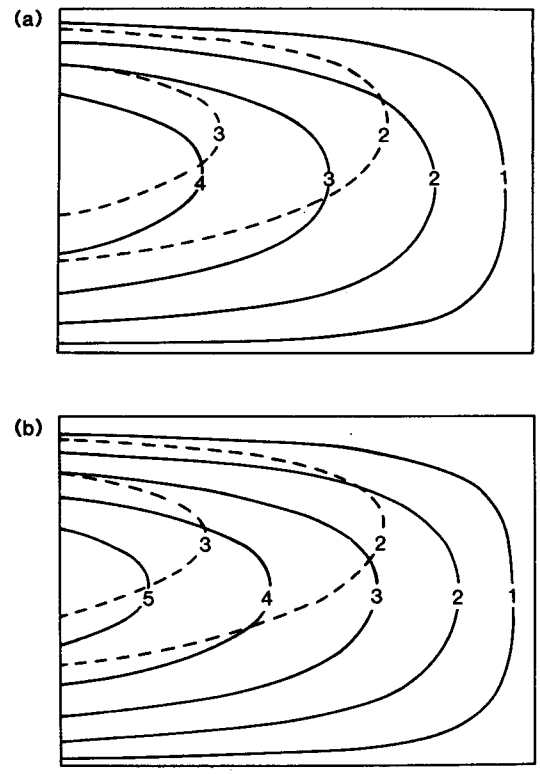

FIG. 13. The perturbation pressure fields at the surface (solid line) and a depth of 500 m (dashed line) [10^3 N m^{-2}] in the subtropical gyre with (a) no mixed layer, and (b) a depth-varying mixed layer.

appears to swing to the west sooner from the increase in the subducted potential vorticity, which is consistent with the heating experiments of Pedlosky (1986). These

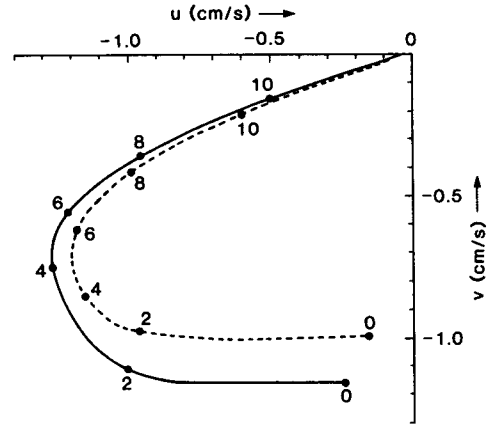

FIG. 14. The beta spiral in the center of the subtropical gyre with the depths marked in units of 200 m over the upper 1 km for (a) no mixed layer (dashed line), and (b) a depth-varying mixed layer (full line).

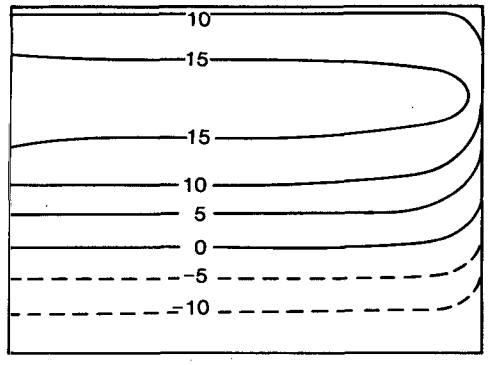

FIG. 15. The implied surface heat flux from the atmosphere into the depth-varying mixed layer [W m^{-2}].

velocity changes correspondingly alter the beta spiral of the flow (Fig. 14).

The surface flow is diabatically modified by the surface heating, which leads to the meridional cross-isopycnal flow within the mixed layer (Fig. 15). The horizontal Ekman flux enhances the southwards geostrophic flux in the northern half of the gyre, but opposes it in the southern half. Consequently, there is an implied surface heating of the cooler water moving south over most of the subtropical gyre, but there is also a cooling of the warmer water forced northwards along the southern edge of the gyre. The implied maximum surface heating of 18 W m^{-2} is consistent with the annual mean climatological observations (Isemer and Hasse 1987), however this may be fortuitous given the simplicity of the ventilation model.

6. Discussion and conclusion

Air–sea interaction influences the ventilation of the main thermocline by making the mixed layer deepen and cool polewards. In the subtropical gyre, ventilated fluid has its potential vorticity set upon leaving the mixed layer and entering the stratified interior. The ventilation of the main thermocline is most influenced by the winter mixed-layer fields, as water-parcels leaving the summer mixed layer tend to be reentrained during the winter mixed-layer deepening. The subducted potential vorticity in the main thermocline is then set by the winter mixed-layer depth and density gradients, as well as by the Ekman pumping, the geostrophic flow and the planetary vorticity. This potential vorticity field helps to determine the baroclinic structure of the gyre, although there will be competition from eddy processes tending to homogenize the potential vorticity. This ventilation mechanism must also be important in controlling the injection of passive tracers, such as CO_2 and tritium, from the mixed layer into the main thermocline. In contrast, the mixed layer is relatively passive in the subpolar gyre, as the Ekman upwelling leads to a flow from the interior into the mixed layer, and the potential vorticity field is set entirely by the western boundary.

A ventilation model is used to assess the influence of an imposed mixed layer on the geostrophic flow in a subtropical gyre. The ventilated fluid passes through the mixed layer and partly originates from the western boundary, as well as from the Ekman layer. In this study, the ratio of the ventilated flow and the total flow into the gyre is increased from O(2/5) for a mixed layer with a uniform thickness to over O(1/2) for a depth-varying mixed layer. The isopycnals are now subducted at much greater depths from the depth-varying mixed layer, and the base of the ventilated layer becomes slightly shallower in compensation, which increases the value of the subducted potential vorticity. However, the potential vorticity change surprisingly only modifies the detail of the general streamline pattern. Instead, the functional relationship between the Montgomery potential and the potential vorticity is substantially changed along each subducted density surface. The increase in the subducted potential vorticity does slightly increase the baroclinic shear, with the surface flow becoming stronger and the deeper flow weaker.

The ventilation model results are strongly constrained by the applied boundary conditions. The imposed mixed-layer depth field is limited by the choice of no inflow on the eastern wall, which requires that the mixed-layer depth vanish there. The density surfaces are also only allowed to outcrop along latitude circles. In reality, there are higher order dynamical balances along the eastern wall producing a more realistic stratification, and the flow may advect the mixed-layer density field leading to a different outcropping pattern. Including these processes that allow a more realistic mixed layer (such as deepening polewards throughout the gyre) may lead to a different subducted potential vorticity field and perhaps larger changes in the baroclinic structure of the gyre.

Acknowledgments. I am grateful to George Nurser and John Marshall for helpful advice and comments. This work was supported by the Admiralty Research Establishment of the United Kingdom.

REFERENCES

Huang, R. X., 1988: On boundary value problems of the ideal-fluid thermocline. *J. Phys. Oceanogr.*, **18**, 619–641.

Isemer, H., and L. Hasse, 1987: The Bunker climate atlas of the North Atlantic Ocean, Vol. 2: Air–sea interaction, Springer-Verlag, 252 pp.

Killworth, P. D., 1987: A continuously stratified nonlinear ventilated thermocline. *J. Phys. Oceanogr.*, **17**, 1925–1943.

Kraus, E. B., and J. S. Turner, 1967: A one-dimensional model of the seasonal thermocline, II. The general theory and its consequences. *Tellus*, **19**, 19–105.

Luyten, J. R., J. Pedlosky and H. Stommel, 1983: The ventilated thermocline. *J. Phys. Oceanogr.*, **13**, 292–309.

Marshall, J. C., and G. Nurser, 1986: Steady free circulation in a quasi-geostrophic ocean. *J. Phys. Oceanogr.*, **16,** 1799–1813.

Niiler, P. P., and P. S. Dubbelday, 1970: Circulation in a wind-swept and cooled ocean. *J. Mar. Res.*, **28,** 135–149.

Pedlosky, J., 1983: Eastern boundary ventilation and the structure of the thermocline. *J. Phys. Oceanogr.*, **13,** 2038–2044.

——, 1986: The buoyancy and wind-driven ventilated thermocline. *J. Phys. Oceanogr.*, **16,** 1077–1087.

——, W. Smith and J. R. Luyten, 1984: On the dynamics of the coupled mixed-layer-thermocline system and the determination of the oceanic surface density. *J. Phys. Oceanogr.*, **14,** 1159–1171.

Rhines, P. B., 1986: Lectures on ocean circulation dynamics. *Large-Scale Transport Processes in Oceans and Atmosphere.* J. Willebrand and D. L. T. Anderson, Eds., D. Reidel.

——, and W. R. Young, 1982: A theory of the wind-driven circulation. I. Mid-ocean gyres. *J. Mar. Res.*, **40**(Suppl.), 559–596.

Robinson, M. K., R. A. Bauer and E. H. Schroeder, 1979: Atlas of North Atlantic–Indian Ocean Monthly Mean Temperature and Mean Salinities of the Surface Layer. U.S. Naval Oceanogr. Office, Washington, DC.

Stommel, H., 1979: Determination of watermass properties of water pumped down from the Ekman layer to the geostrophic flow below. *Proc. Natl. Acad. Sci., U.S.*, **76,** 3051–3055.

Williams, R. G., 1988: Modification of ocean eddies by air–sea interaction. *J. Geophys. Res.*, **93,** 15 523–15 533.

Woods, J. D., 1984: The warm water sphere of the northeast Atlantic: a miscellany. *Ber. Inst. Meereskd. Univ. Kiel,* **128,** 39 pp.

——, 1985: Physics of thermocline ventilation. *Coupled Atmosphere-Ocean Models.* J. C. J. Nihoul, Ed., Elsevier.

——, and W. Barkmann, 1986: The response of the upper ocean to solar heating, I. *Q. J. R. Meteorol. Soc.*, **112,** 1–27.

——, and ——, 1988: A Lagrangian mixed-layer model of Atlantic 18°C water formation. *Nature,* **319,** 574–576.